ISSN 0036-0295, Russian Metallurgy (Metally), Vol. 2020, No. 12, pp. 1439–1445. © Pleiades Publishing, Ltd., 2020.
Russian Text © The Author(s), 2020, published in Elektrometallurgiya, 2020, No. 9, pp. 22–29.

QUALITY, CERTIFICATION, AND COMPETITIVE ABILITY OF METAL PRODUCTS

Structure, Phase Composition, and Mechanical Properties of a Boron-Containing High-Nitrogen Austenitic Steel Made by Induction Melting

I. O. Bannykh[a], *, O. A. Bannykh[a], L. G. Rigina[a], E. N. Blinova[b], K. Yu. Demin[a], and I. N. Lukina[a]

[a] *Baikov Institute of Metallurgy and Materials Science, Russian Academy of Sciences, Moscow, 119335 Russia*

[b] *Bardin Central Research Institute for Ferrous Metallurgy, Moscow, 105005 Russia*

**e-mail: igorbannykh@gmail.com*

Received May 10, 2020; revised May 15, 2020; accepted May 20, 2020

Abstract—The structure and the mechanical properties of a cast high-nitrogen austenitic steel are studied after hot and cold deformation. The as-cast steel contains the FeCrB and BN phases. During hot deformation, the $B_{13}N_{13}C_{74}$ phase forms. This phase has a layered structure and is easily deformed during hot or cold rolling. The existence of the $B_{13}N_{13}C_{74}$ phase only slightly changes the strength and the ductility, but it substantially decreases the impact toughness of the steel as compared to that of similar boron-free Cr–Mn–Ni high-nitrogen austenitic steels.

Keywords: high-nitrogen austenitic steel, boron, boron carbonitride, porosity, strength, ductility, impact toughness

DOI: 10.1134/S003602952012006X

INTRODUCTION

The alloying of austenitic steels with boron is considered as a method to increase the wear [1], cavitation [2], and radiation resistance [3, 4] of austenitic steels. The main methods of its introduction are the deposition of boron-containing coatings [2] or the use of powder metallurgy methods [5, 6]. The limitation of boron alloying of wrought steels is the existence of the FeB + B eutectic in the temperature range of hot deformation. However, the boron alloying of high-nitrogen austenitic steels is assumed to minimize the eutectic formation by fixing boron into nitride (carbonitride) phases and, thus, to increase the ability of steel to hot deformation.

EXPERIMENTAL

The steel of the composition given in Table 1 was melted from pure charge components in a 50-kg induction furnace. The nitrogen concentration was calculated by the formula in [7].

The chemical composition of the steel of the experimental heat is as follows (wt %):

0.01–0.04 C; 0.60–0.72 N; 0.10–0.15 B;

21.0–22.0 Cr; 14.0–15.0 Mn;

3.0–3.5 Ni; <0.3 Si; <0.01 S; <0.02 P.

The charge components were nitrided ferrochromium with 8.7% nitrogen, Armco iron, Kh99 metallic chromium, MRO electrolytic manganese, N1 electrolytic nickel, SK25 silicocalcium with 25% calcium, FS 75 ferrosilicium, FBn 20 ferroboron, and MTs 50ZhZ rare-earth metals (REMs).

A 1 : 1 mixture of calcium hydroxide and fluorspar was used as a slag-forming mixture.

Iron, chromium, and nickel were charged. After melting, the metal was deoxidized with ferrosilicium, manganese was added, the metal was held for 5–6 min and deoxidized with silicocalcium, and ferroboron was added. We measured the melt temperature (1520°C) and added nitrided ferrochromium. After

Table 1. Composition of the steel

Composition	Content of elements								
	C	N	B	Cr	Mn	Ni	Si	S	P
wt %	0.024	0.78	0.11	22.2	14.41	3.5	0.33	0.005	0.003
at %	0.11	2.96	0.54	22.70	13.95	3.17	2.96	0.01	0.01

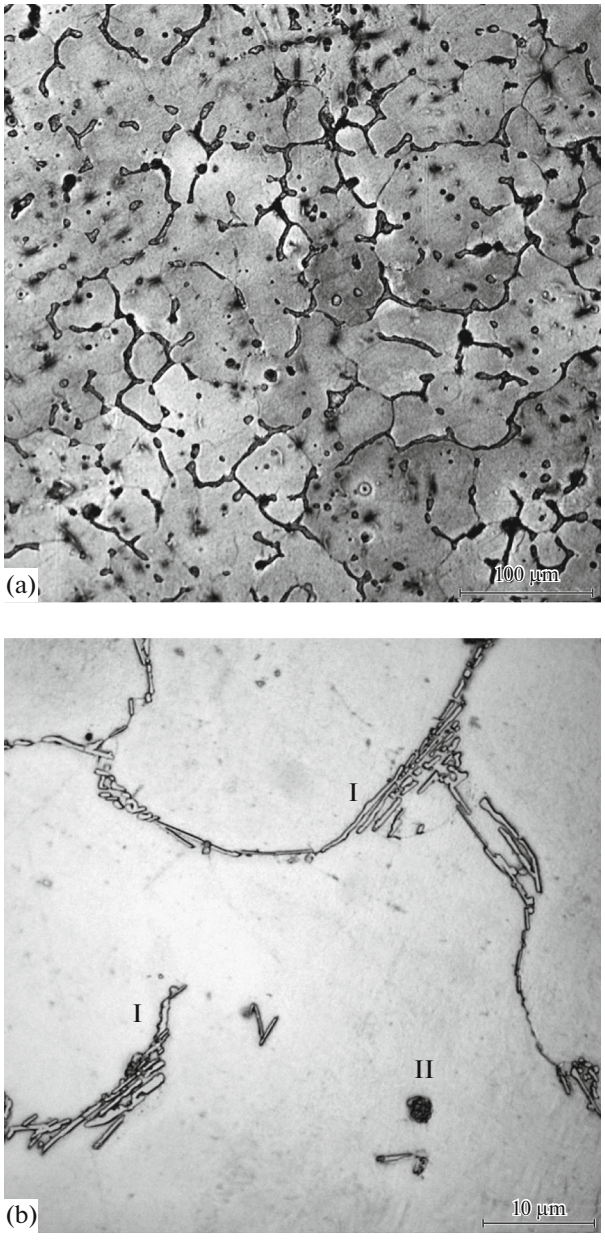

Fig. 1. Structure of the cast metal in (a) as-cast state and (b) after homogenizing annealing at 1200°C for 1 h.

the assimilation of the alloying elements, a slag was discharged. The final deoxidation was performed with silicocalcium in a ladle. The metal temperature was again measured (metal temperature before pouring must be in the range 1500–1540°C). It was 1520°C. The metal was then poured into a ladle. The final deoxidation was performed with REMs in the ladle. We took samples for chemical and gas analyses and poured the metal into a 12-kg crucible and a mold. The mold for casting a billet of a given size was prepared in advance, and its surface was coated by a special-purpose anti-burning coating to decrease the amount of burn-on sand.

After metal solidification, the ingot and the casting were stripped and their surface quality was estimated. We found that the ingot and the casting surfaces have a good quality.

After cutting the head part and visual examination, we noted that the metal was dense and did not have solidification defects.

The ingot was forged in the temperature range 1200–950°C with intermediate heating to a reduction of 25%. To prepare specimens for tensile tests according to GOST 1497 and for bending impact tests according to GOST 9454, the billet was subjected to hot rolling at temperatures 1150–950°C with intermediate heating and finished cooling in water. From the forging piece, we also cut workpieces for hot deformation by rolling with various degrees of reduction.

Tensile tests were carried out on an INSTRON 3382 tensile testing machine. Bending impact tests were carried out on a ZWICK ROELL RKP 450 impact testing machine. Electron-microscopic studies were performed on a LEO-430i scanning electron microscopy, a Jeol JAMP-9500f Auger microanalyzer, and a JEM-200C transmission electron microscope at an accelerating voltage of 160 kV. X-ray diffraction (XRD) analysis was performed on a DRON-7 diffractometer using filtered Co$K\alpha$ radiation. The microhardness was measured using a Shimidzu DUH-211 ultramicrohardness tester.

RESULTS AND DISCUSSION

Figure 1 shows the structure of the as-cast metal. In the initial state, there is a typical dendrite structure with the precipitation of a secondary phase along dendrite arms and grain boundaries (Fig. 1a). The grain size in the as-cast metal is varied in the wide range 20–500 μm. Homogenizing annealing at 1200°C for 1 h did not cause complete dissolution of secondary phases (see Fig. 1b). The phases of two types are determined: (I) a lamellar phase, supposedly, FeCrB, arranged along grain boundaries [2]; local X-ray spectral analysis shows that this phase contains boron, is enriched in chromium, and is depleted of nickel as compared to the base metal (Table 2); (II) a globular phase containing nitrogen and boron, supposedly, boron carbonitride.

The steel is deformed well in the given temperature range. After hot rolling, the ferrite phase and the FeCrB phase are not observed in the steel, but there are significant amounts of inclusions elongated in the rolling direction (Fig. 2a). These inclusions are ductile, their length is up to 100 μm, and the cross-section size is less 1 μm. They are not crack nuclei due to their high plasticity. For example, at 50% cold deformation of the metal annealed at 1100°C, the inclusions disposed along austenite grain boundaries underwent forming without cracking in the surrounding metallic matrix (Fig. 2b). This behavior of the inclusions is

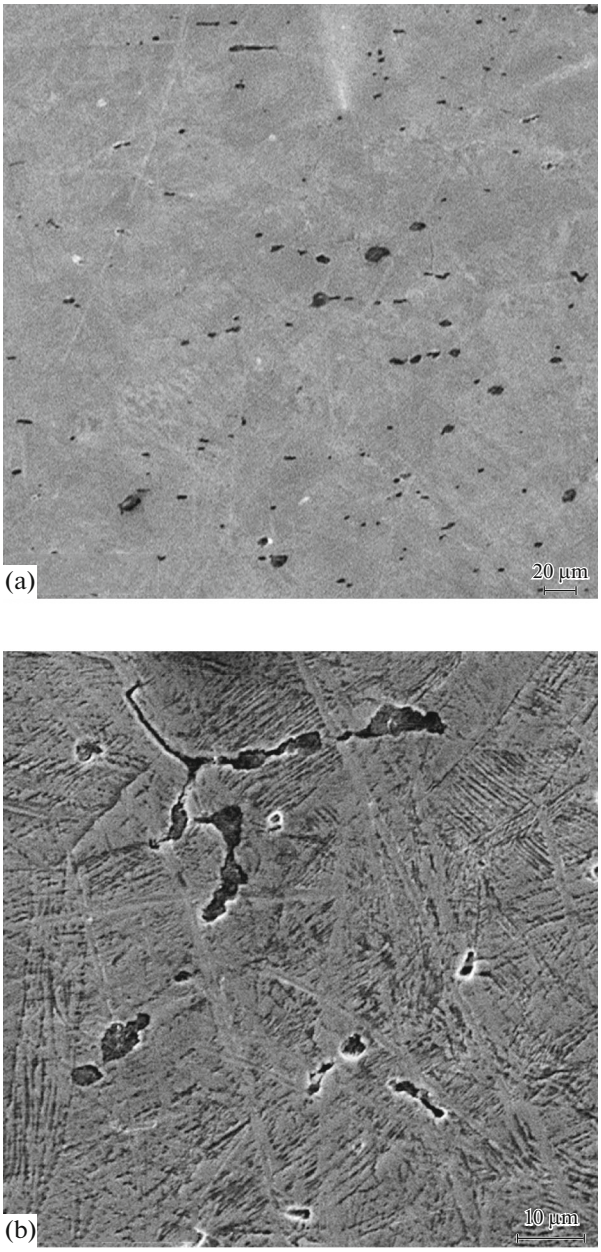

Fig. 2. Structure of the metal after plastic deformation: (a) hot rolling, unetched metallographic section, (b) 50% cold deformation after annealing at 1100°C for 1 h.

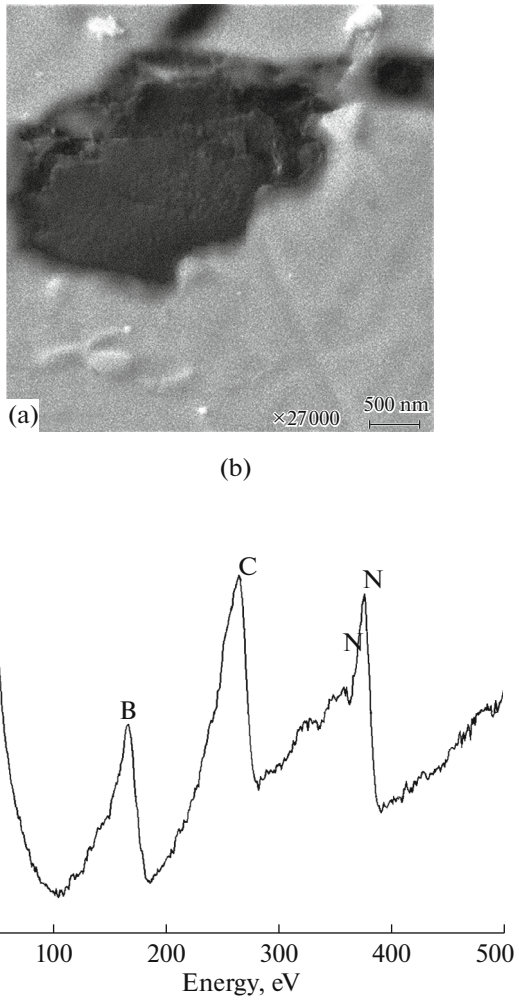

Fig. 3. (a) Layered structure of an inclusion and (b) its Auger spectrum.

related to their morphology: they have a layered structure (Fig. 3a). The layers of thin (~10 nm) films are easily fractured under applied stresses and do not influence the surrounding matrix. They can be considered as pores in the base metal. Auger spectroscopy studies showed the qualitative composition of the inclusions; they consist of nitrogen, boron, and carbon and are likely to be boron carbonitrides (Fig. 3b). The images of a particle (Fig. 4a) and film precipitate (Fig. 4b) of boron carbonitride were taken by transmission electron microscopy. XRD studies identified this phase as $B_{13}N_{13}C_{74}$ (JCPDC 35–192). This phase has the hexagonal crystal lattice with parameters a = 0.2462 nm and c = 0.6790 nm. Based on the atomic

Table 2. Chemical composition of the structural components of the as-cast steel

Structural component	Content of elements, %					
	Cr	Mn	Ni	Si	Fe	B*
Base metal	21.28	15.05	4.01	0.34	59.09	–
FeCrB	43.64	14.26	1.58	0.18	40.34	+

* The boron content was qualitatively determined.

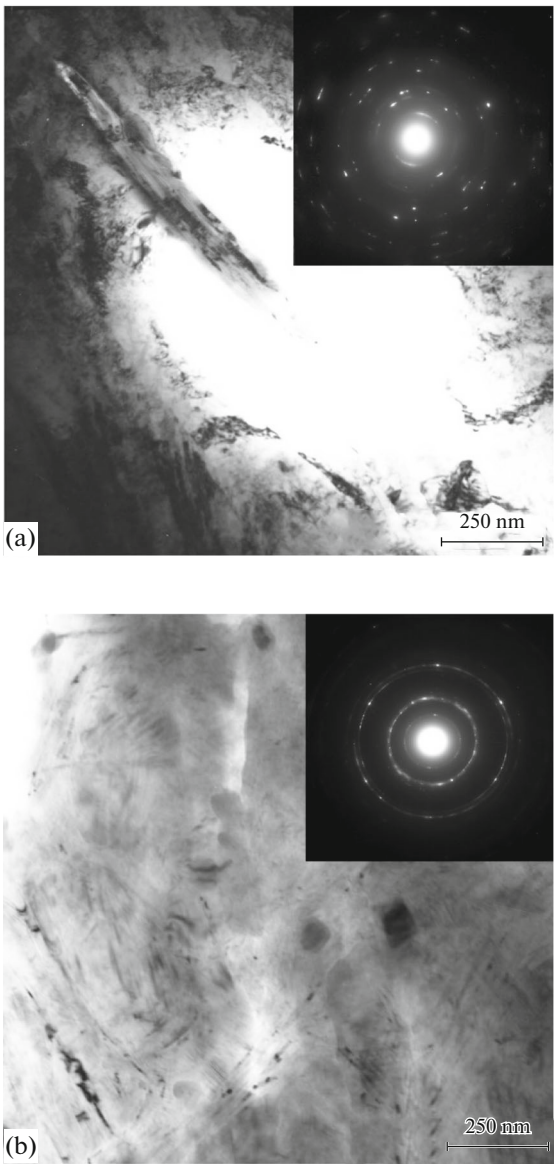

Fig. 4. (a) Boron carbonitride particle and corresponding electron diffraction pattern taken with the (100)-BNC reflection; (b) film precipitate of boron carbonitride and the corresponding electron diffraction pattern taken with the (002)-BNC reflection.

composition of the steel (Table 1) and assuming that almost all carbon is bounded by the carbonitride phase, we find that this phase should contain about 0.02 at % nitrogen and boron from their content in the steel. Thus, we can assume that, under the given heat treatment conditions, a significant part of boron (~0.52 at %) is retained in the solid solution.

The microhardness of the carbonitride phase is low, 74–95 HV at a load of 50.5 mN. An increase in the indentation load leads to the fracture of a carbonitride phase particle and does not enable us to perform measurements. The microhardness of the austenitic matrix is 410–450 HV, which is a quite high value for high-nitrogen austenitic steels after annealing. The modulus of indentation characterizing the elastic properties of the material was 145 GPa for the austenitic matrix and 74.5 GPa for boron carbonitride. The low hardness and elasticity demonstrate that the $B_{13}N_{13}C_{74}$ phase precipitates are likely not to play a positive role in the hardening or an increase in the wear resistance of this steel.

Table 3 lists the mechanical properties of this steel: σ_u is ultimate tensile strength, $\sigma_{0.2}$ is the yield strength, δ is the relative elongation, KCU^{+20} is the impact toughness at room temperature, and KCU^{-196} is the impact toughness at the liquid nitrogen temperature. It should be noted that the steel under study has a high ductility at static loading and a comparatively low

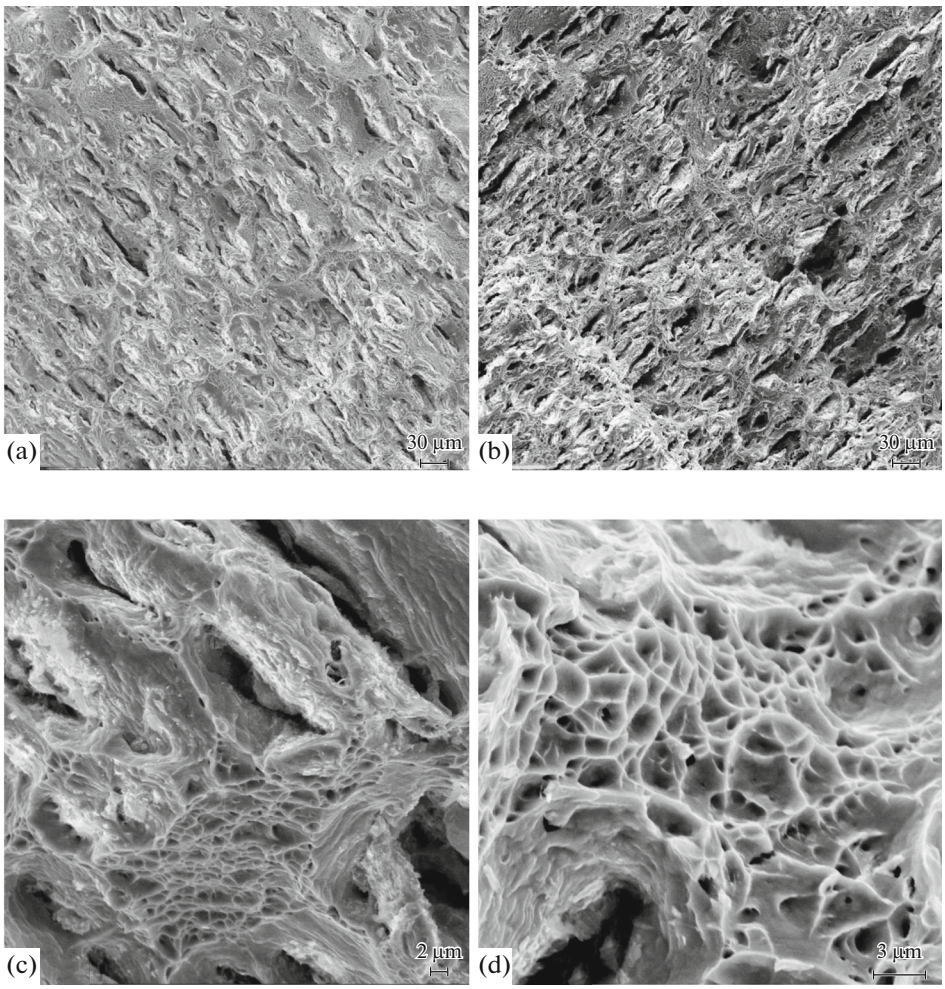

Fig. 5. Fracture surfaces of the steel specimens subjected to static loading: (a, c) hot rolling, (b, d) hot rolling + annealing at 1100°C for 1 h.

impact toughness KCU as compared to those of similar boron-free high-nitrogen austenitic steels [8].

After static loading, the structure of the steel contains pores formed as a result of the spallation of boron carbonitride particles (Figs. 5a, 5b), and the fracture has a plastic character in both the hot-rolled (Fig. 5c) and annealed states (Fig. 5d). In this case, annealing leads to an increase in the number and sizes of carbonitride particles and, as a result, pores.

The fractures after bending impact tests are similar for the hot-rolled and annealed states of the steel (Fig. 6). At room temperature, the fracture is mainly ductile with a wide variation of the fracture dimple sizes from several units to several tens of microns (Figs. 6a, 6b). Large dimples form at the sites of the carbonitride phase. In the impact fracture at the liquid nitrogen temperature, in parallel to the ductile fracture pits, some amount of cleavage facets are observed (Figs. 6c, 6d), which is a common phenomenon for high-nitrogen austenitic steels unlike other fcc alloys undergoing ductile–brittle transition [9]. In the steel subjected to annealing, there are many ductile fracture dimples. The impact toughness is assumed to decrease

Table 3. Mechanical properties of the steel

HT conditions	σ_u, MPa	$\sigma_{0.2}$, MPa	δ, %	KCU^{+20}, MJ/m^2	KCU^{-196}, MJ/m^2
Rolling 1150–950°C	982	712	39.7	0.68	0.28
Rolling + annealing 1100°C 1 h	894	507	60.8	0.98	0.45

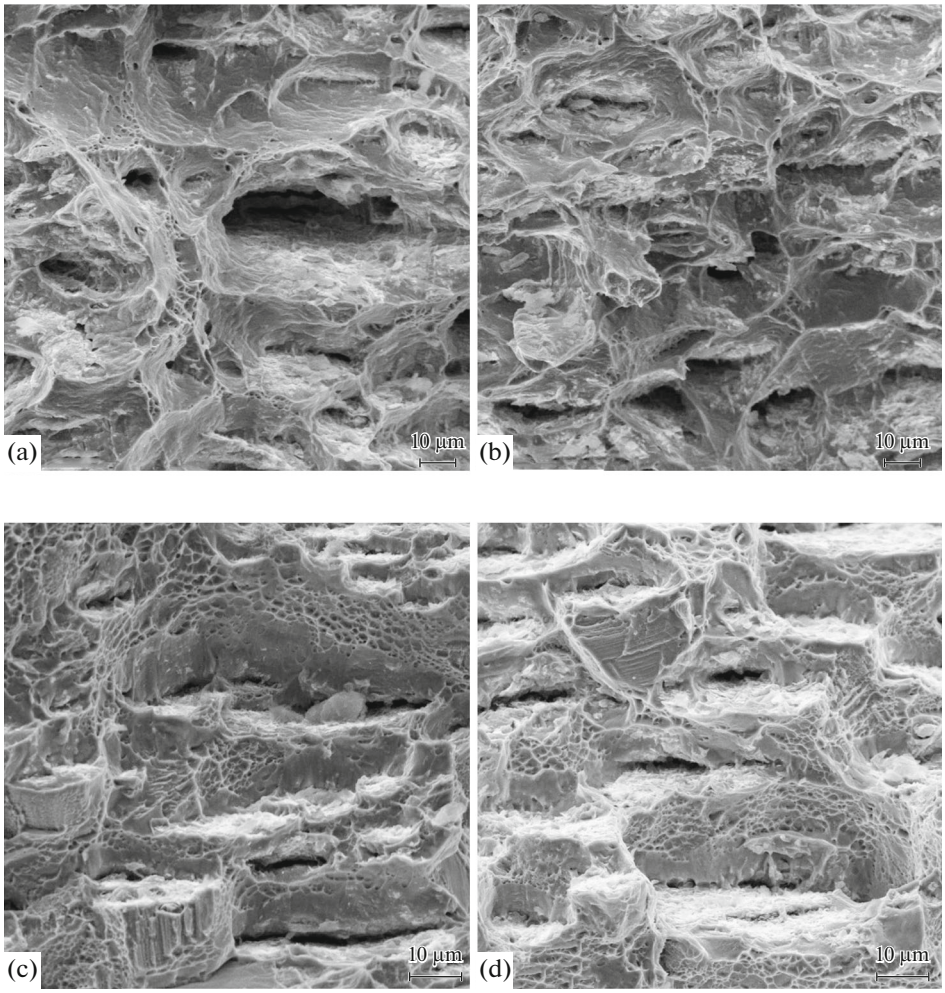

Fig. 6. Fracture surfaces of the steel specimens subjected to bending impact tests at (a, b) 20°C and (c, d) 196°C: (a, c) hot rolling, (b, d) hot rolling + annealing at 1100°C for 1 h.

due to a decrease in the real cross section of the specimen due to the porosity caused by the carbonitride phase.

CONCLUSIONS

The FeCrB and BN phases are detected in as-cast boron-alloyed high-nitrogen steels.

During hot deformation at 1150–950°C, the $B_{13}N_{13}C_{74}$ carbonitride phase with the hcp lattice forms. Based on the content of the alloying elements and the phase composition under experimental conditions, the $B_{13}N_{13}C_{74}$ carbonitride contains insignificant part of the total content of boron in the steel. The main amount of boron is assumed to be in austenite. The $B_{13}N_{13}C_{74}$ phase has a layered structure and is easily deformed during hot and cold plastic deformation of the steel. Because of the extreme low hardness and the elastic properties of the $B_{13}N_{13}C_{74}$ phase, it cannot make a positive contribution to the physicomechanical properties of the steel, forming pores in the austenitic matrix. These pores only slightly decrease the strength and the ductility; however, they substantially decrease the impact toughness of the steel as compared to similar Cr–Mn–Ni boron-free high-nitrogen austenitic steels.

FUNDING

This work is supported by the Ministry of Education and Science of the Russian Federation, state assignment no. 075-00947-20-00.

REFERENCES

1. M. Kulka, D. Mikolajczak, N. Makuch, P. Dziarski, and A. Miclaszewski, "Wear resistance improvement of austenitic 316L steel by laser alloying with boron," Surf. Coat. Technol. **291**, 292–313 (2016). https://doi.org/10.1016/j.surfcoat.2016.02.058
2. J. R. Cruz, S. L. Henke, Anderson G. M. Pukasiewicz, and Ana Sofia C. M. d'Oliveira, "The effect of boron on cavitation resistance of FeCrMnSiB austenitic

stainless steels," Wear **436–437**, 203041 (2019). https://doi.org/10.1016/j.wear2019.203041

3. I. Akkurt, A. Calik, and H. Akyildirim, "The boronizing effect on the radiation shielding and magnetization properties of AISI 316L austenitic stainless steel," Nucl. Eng. Des. **241** (1), 55–58 (2011). https://doi.org/10.1016/j.nucengdes.2010.10.009
4. T. Okita, W. G. Wolfer, F. A. Garner, and N. Sekimura, "Influence of boron on void swelling in model austenitic steels," J. Nucl. Mater. **329–333** (Part B), 1013–1016 (2004). https://doi.org/10.1016/j.jnucmat.2004.04.126
5. F. L. Serafini, M. Peruzzo, I. Krindges, M. F. C. Ordoñez, D. Rodrigues, R. M. Souza, and M. C. M. Farias, "Microstructure and mechanical behavior of 316L liquid phase sintered stainless steel with boron addition," Mater. Char. **152**, 253–264 (2019). https://doi.org/10.1016/j.matchar.2019.04.009
6. M. Peruzzo, T. D. Beux, M. F. C. Ordoñez, R. M. Sonza, and M. C. M. Farias, "High-temperature oxidation of sintered austenitic stainless steel containing boron or yttria," Cor. Sci. **129**, 26–37 (2017).
7. L. G. Rigina, "Study and development of the technology of EShP and EShPD chromium–manganese steels alloyed with nitrogen," Cand. Sci. (Eng.) Dissertation, Moscow, NPO TsNIITMASh, 2005.
8. I. O. Bannykh, "Structural features and perspectives of applying high-nitrogen austenitic steels," Metalloved. Term. Obrab. Met., No. 5, 22–29 (2019).
9. L. R. Botvina, V. M. Blinov, M. R. Tyutin, I. O. Bannykh, and E. V. Blinov, "Fracture of high-nitrogen 05KH20G10N3AMF steel during impact loading," Russ. Metall. (Metally), No. 3, 239–247 (2012).

Translated by Yu. Ryzhkov